

Equivariant Graph Hierarchy-Based Neural Networks

Jiaqi Han¹, Yu Rong², Tingyang Xu², Fuchun Sun¹, Wenbing Huang^{*3}

¹ Beijing National Research Center for Information Science and Technology (BNRist), Department of Computer Science and Technology, Tsinghua University

² Tencent AI Lab, Tencent

³ Institute for AI Industry Research (AIR), Tsinghua University

hanjq21@mails.tsinghua.edu.cn, yu.rong@hotmail.com

tingyangxu@tencent.com, fcsun@mail.tsinghua.edu.cn, hwenbing@126.com

Abstract

Equivariant Graph neural Networks (EGNs) are powerful in characterizing the dynamics of multi-body physical systems. Existing EGNs conduct *flat* message passing, which, yet, is unable to capture the spatial/dynamical hierarchy for complex systems particularly, limiting substructure discovery and global information fusion. In this paper, we propose Equivariant Hierarchy-based Graph Networks (EGHNs) which consist of the three key components: generalized Equivariant Matrix Message Passing (EMMP) , E-Pool and E-UpPool. In particular, EMMP is able to improve the expressivity of conventional equivariant message passing, E-Pool assigns the quantities of the low-level nodes into high-level clusters, while E-UpPool leverages the high-level information to update the dynamics of the low-level nodes. As their names imply, both E-Pool and E-UpPool are guaranteed to be equivariant to meet physic symmetry. Considerable experimental evaluations verify the effectiveness of our EGHN on several applications including multi-object dynamics simulation, motion capture, and protein dynamics modeling.

1 Introduction

Understanding the multi-body physical systems is vital to numerous scientific problems, from microscopically how a protein with thousands of atoms acts and folds in the human body to macroscopically how celestial bodies influence each other's movement. While this is exactly an important form of expert intelligence, researchers have paid attention to teaching a machine to discover the physic rules from the observational systems through end-to-end trainable neural networks. Specifically, it is natural to use Graph Neural Networks (GNNs), which is able to model the relations between different bodies into a graph and the inter-body interaction as the message passing thereon (Battaglia et al., 2016; Kipf et al., 2018; Sanchez-Gonzalez et al., 2019, 2020; Pfaff et al., 2020).

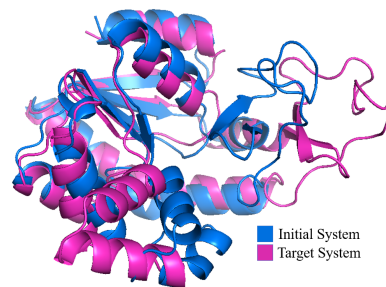


Figure 1: The folding dynamics of proteins in the cartoon format.

*Corresponding author

More recently, Equivariant GNNs (EGNs) (Thomas et al., 2018; Fuchs et al., 2020; Finzi et al., 2020; Satorras et al., 2021) have become a crucial kind of tool for representing multi-body systems. One desirable property is that their outputs are equivariant with respect to any translation/orientation/reflection of the inputs. With this inductive bias encapsulated, EGN permits the symmetry that the physic rules keep unchanged regardless of the reference coordinate system, enabling more enhanced generalization ability. Nevertheless, current EGNs only conduct *flat* message passing in the sense that each layer of message passing in EGN is formulated in the same graph space, where the spatial and dynamical information can only be propagated node-wisely and locally. By this design, it is difficult to discover the hierarchy of the patterns within complex systems.

Hierarchy is common in various domains. Imagine a complex mechanical system, where the particles are distributed on different rigid objects. In this case, for the particles on the same object, their states can be explained as the relative states to the object (probably the center) plus the dynamics of the object itself. We can easily track the behavior of the system if these “implicit” objects are detected automatically by the model we use. Another example, as illustrated in Figure 1, is the dynamics of a protein. Most proteins fold and change in the form of regularly repeating local structures, such as α -helix, β -sheet and turns. By applying a hierarchical network, we are more capable of not only characterizing the conformation of a protein, but also facilitating the propagation between thousands of atoms in a protein by a more efficient means. There are earlier works proposed for hierarchical graph modeling (Hu et al., 2019; Deng et al., 2020; Ying et al., 2018; Cangea et al., 2018; Lee et al., 2019), but these studies focus mainly on generic graph classification, and more importantly, they are not equivariant.

In this paper, we propose Equivariant Graph Hierarchy-based Network (EGHN), an end-to-end trainable model to discover local substructures of the input systems, while still maintaining the Euclidean equivariance. In a nutshell, EGHN is composed of an encoder and a decoder. The encoder processes the input system from fine-scale to coarse-scale, where an Equivariant-Pooling (E-Pool) layer is developed to group the low-level particles into each of a certain number of clusters that are considered as the particles of the next layer. By contrast, the decoder recovers the information from the coarse-scale system to the fine-scale one, by using the proposed Equivariant-Up-Pooling (E-UpPool) layer. Both E-Pool and E-UpPool are equivariant with regard to Euclidean transformations via our specific design. EGHN is built upon a generalized equivariant layer, which passes directional matrices over edges other than passing vectors in EGNN (Satorras et al., 2021).

To verify the effectiveness of EGHN, we have simulated a new task extended from the N-body system (Kipf et al., 2018), dubbed M-complex system, where each of the M complexes is a rigid object comprised of a set of particles, and the dynamics of all complexes are driven by the electromagnetic force between particles. In addition to M-complex, we also carry out evaluations on two real applications: human motion caption (CMU, 2003) and the Molecular Dynamics (MD) of proteins (Seyler & Beckstein). For all tasks, our EGHN outperforms state-of-the-art EGN methods, indicating the efficacy and necessity of the proposed hierarchical modeling idea.

2 Related Work

GNNs for modeling physical interaction. Graph Neural Networks have been widely investigated for modeling physical systems with multiple interacting objects. As pioneer attempts, Interaction Networks (Battaglia et al., 2016) have been introduced to reason about the physical interactions, NRI (Kipf et al., 2018) conducts relational inference for the system in a variational manner, and HRN (Mrowca et al., 2018) further facilitates the prediction of complex dynamical systems by manually grouping the particles. With the development of neural networks enforced by physical priors, many works resort to injecting physical knowledge into the design of GNNs. As an example, inspired by HNN (Greydanus et al., 2019), HOGN (Sanchez-Gonzalez et al., 2019) models the evolution of interacting systems by Hamiltonian equations to obtain energy conservation. Another interesting physical property is equivariance, and particularly, the Euclidean equivariance, which prevails in the physical world. To this end, several works tackle translation equivariance (Ummenhofer et al., 2019; Sanchez-Gonzalez et al., 2020; Pfaff et al., 2020). TFN (Thomas et al., 2018) and SE(3)-Transformer (Fuchs et al., 2020) leverages the irreducible representation of the SO(3) group, while LieConv (Finzi et al., 2020) and LieTransformer (Hutchinson et al., 2021) employs the regular representation with Lie algebra, to achieve rotation equivariance. Aside from the representation theory, a succinct equivariant message passing scheme on E(n) group is depicted in EGNN (Satorras

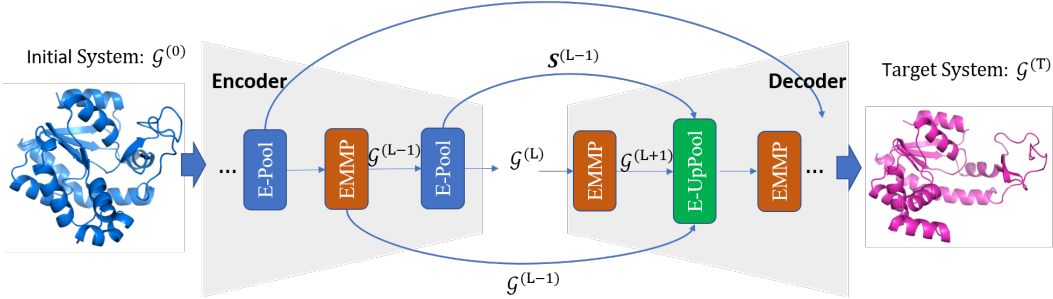


Figure 2: Illustration of the proposed EGHN. It consists of an encoder and a decoder, which are equipped with E-Pool and E-UpPool, respectively. For E-UpPool, it takes as the input the output of the previous layer as well as the score matrix S from E-Pool and the low-level system \mathcal{G} in the corresponding layers of the encoder. There always one EMMP layer prior to E-Pool/E-UpPool.

et al., 2021). Following this approach, GMN (Huang et al., 2022) further involves forward kinematics modeling particularly for constrained systems. Despite the rich literature, these models either inspect the system at a single granularity, or violate the equivariance, both of which are crucial aspects to consider especially when tackling highly complicated systems like proteins.

Conventional Hierarchical GNNs. There are also works that explore the representation learning of GNNs in a hierarchical fashion. Several GNNs (Hu et al., 2019; Deng et al., 2020; Xing et al., 2021) adopt graph coarsening algorithms to view the graph in multiple granularities. Another line of work injects learnable pooling modules into the model. A differentiable pooling scheme DiffPool (Ying et al., 2018) has been introduced to learn a permutation-invariant pooling in an end-to-end manner. Cangea et al. (2018) replaces the aggregation in DiffPool by node dropping for saving the computational cost. Lee et al. (2019) further incorporates self-attention mechanism into the pooling network. Nevertheless, these pooling techniques lack the guarantee of equivariance, which limits their application on physical data. In addition, they only consider the bottom-up pooling process while the top-down update has not been elaborated.

3 The Proposed EGHN

In this section, we first introduce the notations and formulation of our task, and then follow them up by presenting the design of the EMMP layer, which is the basic function in EGHN. Upon EMMP, we provide the details of how the proposed E-Pool and E-UpPool work. Finally, we describe the instantiation of the entire architecture.

3.1 Notations and Formulation

Each input multi-body system is modeled as a graph \mathcal{G} consisting of N particles (nodes) \mathcal{V} and the interactions (edges) \mathcal{E} among them. For each node i , it is assigned with a feature tuple $(\mathbf{Z}_i^{(0)}, \mathbf{h}_i^{(0)})$, where the directional matrix $\mathbf{Z}_i^{(0)} \in \mathbb{R}^{n \times m}$ is composed of m n -dimension vectors, such as the concatenation of position $\mathbf{x}_i \in \mathbb{R}^3$ and velocity $\mathbf{v}_i \in \mathbb{R}^3$; $\mathbf{h}_i \in \mathbb{R}^c$ is the non-directional feature, such as the category of the atom in molecules. The edges are represented by an adjacency matrix $\mathbf{A} \in \mathbb{R}^{N \times N}$. We henceforth abbreviate the entire information of a system, *i.e.*, $(\{\mathbf{Z}_i^{(0)}, \mathbf{h}_i^{(0)}\}_{i=1}^N, \mathbf{A})$ as the notation \mathcal{G}^{in} if necessary.

We are mainly interested in investigating the dynamics of the input system \mathcal{G}^{in} . To be formal, starting from the initial state $(\mathbf{Z}_i^{(0)}, \mathbf{h}_i^{(0)})$ of each particle, our task is to find out a function ϕ to predict its future state $\mathbf{Z}_i^{(T)}$ given the interactions between particles. As explored before (Thomas et al., 2018; Fuchs et al., 2020; Finzi et al., 2020; Satorras et al., 2021), ϕ is implemented as a GNN to encode the inter-particle relation. In addition, it should be equivariant to any translation/reflection/rotation of the input states, so as to obey the physics symmetry about the coordinates. It means, $\forall g \in E(n)$ that

defines the Euclidean group (Satorras et al., 2021),

$$\phi(\{g \cdot \mathbf{Z}_i^{(0)}\}_{i=1}^N, \dots) = g \cdot \phi(\{\mathbf{Z}_i^{(0)}\}_{i=1}^N, \dots), \quad (1)$$

where $g \cdot \mathbf{Z}_i^{(0)}$ conducts the orthogonal transformation as $\mathbf{R}\mathbf{Z}_i^{(0)}$ for both the position and velocity vectors and is additionally implemented as the translation $\mathbf{x}_i + \mathbf{b}$ for the position vector; the ellipsis denotes the input variables uninfluenced by g , including $\mathbf{h}_i^{(0)}$ and \mathbf{A} .

As discussed in Introduction, existing equivariant models (Thomas et al., 2018; Fuchs et al., 2020; Finzi et al., 2020; Satorras et al., 2021) are unable to mine the hierarchy within the dynamics of the input system by flat message passing. To address this pitfall, EGHN is formulated in the encoder-decoder form:

$$\mathcal{G}^{\text{high}} = \text{Encode}(\mathcal{G}^{\text{in}}), \quad (2)$$

$$\mathcal{G}^{\text{out}} = \text{Decode}(\mathcal{G}^{\text{high}}, \mathcal{G}^{\text{in}}). \quad (3)$$

Here, as illustrated in Figure 2, the encoder aims at clustering the particles of \mathcal{G}^{in} with similar dynamics into a group that is treated as the particle in the high-level graph $\mathcal{G}^{\text{high}}$ (the number of the nodes in $\mathcal{G}^{\text{high}}$ is smaller than \mathcal{G}^{in}). We have developed a novel component, E-Pool to fulfill this goal. As for the decoder, it recovers the information of all particles in the original graph space under the guidance of the high-level system $\mathcal{G}^{\text{high}}$, which is accomplished by the proposed E-UpPool. It is worth mentioning that both E-Pool and E-UpPool, as their names imply, are equivariant, and they are mainly built upon an expressive and generalized equivariant message passing layer, EMMP. To facilitate the understanding of our model, we first introduce the details of this layer in what follows.

3.2 Equivariant Matrix Message Passing

Given input features $\{(\mathbf{Z}_i, \mathbf{h}_i)\}_{i=1}^N$, EMMP performs information aggregation on the same graph to obtain the new features $\{(\mathbf{Z}'_i, \mathbf{h}'_i)\}_{i=1}^N$. The dimension of the output features could be different from the input, unless the row dimension of \mathbf{Z}'_i should keep the same as \mathbf{Z}_i (*i.e.* equal to n). In detail, one EMMP layer is updated by

$$\mathbf{H}_{ij} = \text{MLP}\left(\hat{\mathbf{Z}}_{ij}^\top \hat{\mathbf{Z}}_{ij}, \mathbf{h}_i, \mathbf{h}_j\right), \quad (4)$$

$$\mathbf{M}_{ij} = \hat{\mathbf{Z}}_{ij} \mathbf{H}_{ij}, \quad (5)$$

$$\mathbf{h}'_i = \text{MLP}(\mathbf{h}_i, \sum_{j \in \mathcal{N}(i)} \mathbf{H}_{ij}), \quad (6)$$

$$\mathbf{Z}'_i = \mathbf{Z}_i + \sum_{j \in \mathcal{N}(i)} \mathbf{M}_{ij}, \quad (7)$$

where $\text{MLP}(\cdot)$ is a Multi-Layer Perceptron, $\mathcal{N}(i)$ collects the neighbors of i , and $\hat{\mathbf{Z}}_{ij} = (\mathbf{Z}_i - \bar{\mathbf{Z}}, \mathbf{Z}_j - \bar{\mathbf{Z}})$ is a concatenation of the translated matrices on the edge ij . $\bar{\mathbf{Z}}$ is the mean of all nodes for the position vectors and zero for other vectors. With the subtraction of $\bar{\mathbf{Z}}$, $\hat{\mathbf{Z}}_{ij}$ is ensured to be translation invariant, and then \mathbf{Z}'_i is translation equivariant after the addition of \mathbf{Z}_i in Eq. 7. Overall, it is easy to justify that EMMP is equivariant *w.r.t.* E(n).

Distinct from EGNN (Satorras et al., 2021), the messages to pass in EMMP are directional matrices other than vectors. Although GMN (Huang et al., 2022) has also explored the matrix form, it is just a specific case of our EMMP by simplifying $\hat{\mathbf{Z}}_{ij} = \mathbf{Z}_i - \mathbf{Z}_j$. Actually, EMMP can be degenerated to either EGNN or GMN by certain relaxations. Also, similar to EGNN, we can replace Eq. 7 with a recursive form by, for instance, first updating the velocity \mathbf{v}_i and then the position \mathbf{x}_i when $\mathbf{Z}_i = [\mathbf{x}_i, \mathbf{v}_i]$, which is exactly the case in our experimental implementation.

3.3 Equivariant Pooling

The role of E-Pool is to coarsen the low-level system $\mathcal{G}^{\text{low}} = (\{(\mathbf{Z}_i^{\text{low}}, \mathbf{h}_i^{\text{low}})\}_{i=1}^N, \mathbf{A}^{\text{low}})$ into an abstract and high-level system $\mathcal{G}^{\text{high}} = (\{(\mathbf{Z}_i^{\text{high}}, \mathbf{h}_i^{\text{high}})\}_{i=1}^K, \mathbf{A}^{\text{high}})$ with fewer particles, $K < N$. For this purpose, we first perform EMMP (Eq. 4-7) over the input system \mathcal{G} to capture the local topology of each node. Then we apply the updated features of each node to predict which cluster it

belongs to. This can be realized by a SoftMax layer to output a soft score for each of the K clusters. The cluster is deemed as a node of the high-level system, and its features are computed as a weighted combination of the low-level nodes with the scores it just derives. In summary, we proceed the following equations:

$$\{\mathbf{Z}'_i, \mathbf{h}'_i\}_i^N = \text{EMMP}(\{\mathbf{Z}_i^{\text{low}}, \mathbf{h}_i^{\text{low}}\}_i^N, \mathbf{A}^{\text{low}}), \quad (8)$$

$$\mathbf{s}_i = \text{SoftMax}(\text{MLP}(\mathbf{h}'_i)), \quad (9)$$

$$\mathbf{Z}_j^{\text{high}} = \frac{1}{\sum_{i=1}^N s_{ij}} \sum_{i=1}^N s_{ij} \mathbf{Z}'_i, \quad (10)$$

$$\mathbf{h}_j^{\text{high}} = \frac{1}{\sum_{i=1}^N s_{ij}} \sum_{i=1}^N s_{ij} \mathbf{h}_i^{\text{low}}, \quad (11)$$

$$\mathbf{A}^{\text{high}} = \mathbf{S}^{\top} \mathbf{A}^{\text{low}} \mathbf{S}, \quad (12)$$

where the score matrix is given by $\mathbf{S} = [s_{ij}]_{N \times K}$, and \mathbf{s}_i is its i -th row.

By the above design, it is tractable to verify that E-Pool is guaranteed to be E(n) equivariant (also permutation equivariant). Specifically, the division by the row-wise sum $\sum_{i=1}^N s_{ij}$ in Eq. 10 is essential, as it permits the translation equivariance, that is, $\frac{1}{\sum_{i=1}^N s_{ij}} \sum_{i=1}^N s_{ij} (\mathbf{Z}'_i + \mathbf{b}) = \left(\frac{1}{\sum_{i=1}^N s_{ij}} \sum_{i=1}^N s_{ij} \mathbf{Z}'_i \right) + \mathbf{b}$. This particular property distinguishes our pooling from traditional non-equivariant graph pooling (Ying et al., 2018; Lee et al., 2019). Notice that the normalization in Eq. 11 is unnecessary since \mathbf{h}_i is a non-directional vector, but it is still adopted in line with Eq. 10. In practice, it is difficult to attain desirable clusters by using the SoftMax layer solely; instead, the pooling results are enhanced if we regulate the training process with an extra reconstruction loss related to the score matrix, whose formulation will be given in § 3.5.

3.4 Equivariant UpPooling

E-UpPool maps the information of the high-level system $\mathcal{G}^{\text{high}}$ back to the original system space \mathcal{G}^{low} , leading to an output system \mathcal{G}^{out} . We project the features back to the space of the original low-level system by using the transposed scores derived in E-Pool. Then, the projected features along with the low-level features are integrated by an E(n) equivariant function to give the final output. Particularly,

$$\mathbf{Z}_i^{\text{agg}} = \sum_{j=1}^K s_{ij} \mathbf{Z}_j^{\text{high}}, \quad (13)$$

$$\mathbf{h}_i^{\text{agg}} = \sum_{j=1}^K s_{ij} \mathbf{h}_j^{\text{high}}, \quad (14)$$

$$\mathbf{h}_i^{\text{out}} = \text{MLP}(\hat{\mathbf{Z}}_i^{\top} \hat{\mathbf{Z}}_i, \mathbf{h}_i^{\text{low}}, \mathbf{h}_i^{\text{agg}}), \quad (15)$$

$$\mathbf{Z}_i^{\text{out}} = \hat{\mathbf{Z}}_i \mathbf{h}_i^{\text{out}}, \quad (16)$$

where $\hat{\mathbf{Z}}_i = [\mathbf{Z}_i^{\text{low}} - \bar{\mathbf{Z}}^{\text{low}}; \mathbf{Z}_i^{\text{agg}} - \bar{\mathbf{Z}}^{\text{agg}}]$ is the column-wise concatenation of the mean-translated low-level matrix $\mathbf{Z}_i^{\text{low}}$ and the high-level matrix $\mathbf{Z}_i^{\text{agg}}$, analogous to Eq. 4. One interesting point is that Eq. 14 is naturally equivariant in terms of translations, even without the normalization term used in Eq. 10. This is because the score matrix is summed to 1 for each row, indicating that $\sum_{j=1}^K s_{ij} (\mathbf{Z}_j^{\text{high}} + \mathbf{b}) = \sum_{j=1}^K s_{ij} \mathbf{Z}_j^{\text{high}} + \mathbf{b}$.

3.5 Instantiation of the Architecture

Figure 2 depicts the instantiation of the whole architecture. The encoder is equipped with a certain number of E-Pools and EMMPs, while the decoder is realized with E-UpPools and EMMPs. For each E-UpPool in the decoder, as already defined in § 3.4, it is fed with the output of the previous layer, the score matrix \mathbf{S} from E-Pool, and the low-level system \mathcal{G} from EMMP in the corresponding layers of the encoder. Here, the so-called corresponding layers in E-Pool and E-UpPool are referred

Table 1: Prediction error ($\times 10^{-2}$) on various types of simulated datasets. The “Multiple System” contains $J = 5$ different systems. For each column, $(M, N/M)$ indicates that each system contains M complexes of average size N/M . Results averaged across 3 runs. “OOM” denotes out of memory.

	Single System				Multiple Systems			
	(3, 3)	(5, 5)	(5, 10)	(10, 10)	(3, 3)	(5, 5)	(5, 10)	(10, 10)
Linear	35.15 ± 0.01	35.22 ± 0.00	30.14 ± 0.00	31.44 ± 0.01	35.91 ± 0.01	35.29 ± 0.01	30.88 ± 0.01	32.49 ± 0.01
TFN	25.11 ± 0.15	29.35 ± 0.17	26.01 ± 0.22	OOM	27.33 ± 0.21	29.01 ± 0.13	25.57 ± 0.14	OOM
SE(3)-Tr.	27.12 ± 0.26	28.87 ± 0.09	24.48 ± 0.35	OOM	28.14 ± 0.16	28.66 ± 0.10	25.00 ± 0.28	OOM
GNN	16.00 ± 0.11	17.55 ± 0.19	16.15 ± 0.08	15.91 ± 0.15	16.76 ± 0.13	17.58 ± 0.11	16.55 ± 0.21	16.05 ± 0.16
RF	14.20 ± 0.09	18.37 ± 0.12	17.08 ± 0.03	18.57 ± 0.30	15.17 ± 0.10	18.55 ± 0.12	17.24 ± 0.11	19.34 ± 0.25
EGNN	12.69 ± 0.19	15.37 ± 0.13	15.12 ± 0.11	14.64 ± 0.27	13.33 ± 0.12	15.48 ± 0.16	15.29 ± 0.12	15.02 ± 0.18
EGHN	11.58 ± 0.01	14.42 ± 0.08	14.29 ± 0.40	13.09 ± 0.66	12.80 ± 0.56	14.85 ± 0.03	14.50 ± 0.08	13.11 ± 0.92

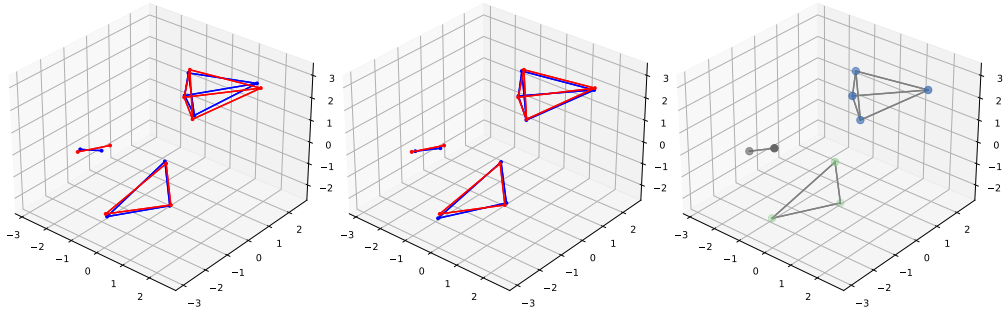


Figure 3: Visualization on M-complex systems. *Left*: the prediction of EGNN. *Middle*: the prediction of EGHN. *Right*: the pooling results of EGHN with each color indicating a cluster. In the left and middle figure, ground truth in red, and prediction in blue. Best viewed by colour printing.

to the ones arranged in an inverse order; for example, in Figure 2, the final E-Pool corresponds to the first E-UpPool.

There is always one EMMP layer prior to each E-Pool or E-UpPool. This external EMMP plays a different role from the internal EMMP used in E-Pool (Eq. 8). One crucial difference is that they leverage different adjacency matrices. **1.** The external EMMP exploits A_{global} whose element is valued if the distance between two particles is less than a threshold; by such means, we are able to characterize the force interaction between any two particles even they are physically disconnected. In higher-layer external EMMP, its A_{global} is created as a re-scored form (akin to Eq. 12) of A_{global} in lower layer, where the score matrix is obtained by its front E-Pool. **2.** For the internal EMMP in E-Pool, it applies A_{local} that exactly reflects the physical connection between particles, for example, it is valued 1 if there is a bond between two atoms. In this way, E-Pool pays more attention to locally-connected particles when conducting clustering. Another minor point is that the external EMMP is relaxed as EGNN for only modeling the radial interaction, whereas the internal EMMP uses the generalized form in § 3.2.

The training objective of EGHN is given by:

$$\mathcal{L} = \sum_{i=1}^N \|\mathbf{Z}_i^{\text{out}} - \mathbf{Z}_i^{\text{gt}}\|_F^2 + \lambda \sum_{l=1}^L \|(\mathbf{S}^{(l)})^\top \mathbf{A}^{(l-2)} \mathbf{S}^{(l)} - \mathbf{I}\|_F^2, \quad (17)$$

where $\|\cdot\|_F$ computes the Frobenius norm, L is the number of E-Pools in the encoder, and λ is the trade-off weight. The first term is to minimize the mean-square-error between the output state $\mathbf{Z}_i^{\text{out}}$ and the ground truth \mathbf{Z}_i^{gt} . The second term is the connectivity loss that encourages more connects within the pooling nodes and less cuts among pooling clusters (Yu et al., 2020). For training stability, we first perform row-wise normalization of $(\mathbf{S}^{(l)})^\top \mathbf{A}^{(l-2)} \mathbf{S}^{(l)}$ before substituting it into Eq. 17.

4 Experiments

We contrast the performance of the proposed EGHN against a variety of baselines including the equivariant and non-equivariant GNNs, on one simulation task: the M-complex system, and the two real-world applications: human motion capture and molecular dynamics on proteins. We also carry out a complete set of ablation studies to verify the optimal design of our model.

4.1 Simulation Dataset: M-complex System

Data generation. We extend the N-body simulation system from Kipf et al. (2018) and generate the M-complex simulation dataset. Specifically, we initialize a system with N charged particles $\{\mathbf{x}_i, \mathbf{v}_i, c_i\}_{i=1}^N$ distributed on M disjoint complex objects $\{\mathcal{S}_j\}_{j=1}^M$, where $\mathbf{x}_i, \mathbf{v}_i, c_i$ are separately the position, velocity, and charge for each particle. Within each complex \mathcal{S}_j , the particles are connected by rigid sticks, yielding sticks, triangles, etc. The dynamics of all M complexes are driven by the electromagnetic force between every pair of particles. The task here is to predict the final positions $\{\mathbf{x}_i^T\}_{i=1}^N$ of all particles when $T = 1500$ given their initial positions and velocities. Without knowing which complex each particle belongs to, we will also test if our EGHN can group the particles correctly just based on the distribution of the trajectories. We construct J different systems with varying combinations of different kinds of complexes to better justify the generation ability of the compared methods. Therefore, a dataset consists J systems with M complexes, N/M average size of complex is abbreviated as $(M, N/M, J)$. We adopt Mean Squared Error (MSE) as the evaluation metric for the experiments.

Implementation details. We assign the node feature as the norm of the velocity $\|\mathbf{v}_i\|_2$, and the edge attribute as $c_i c_j$ for the edge connecting node i and j , following the setting in Satorras et al. (2021). We also concatenate an indicator, which is set as 1 if a stick presents and 0 otherwise, to the edge feature, similar to Huang et al. (2022). We use a fully connected graph (without self-loops) as $\mathbf{A}_{\text{global}}$, since the interaction force spans across each pair of particles in the system. The adjacency matrix \mathbf{A} reflects the connectivity of the particles formed by the complexes. We set the number of clusters the same as the number of complexes in the dataset. The detailed hyper-parameter settings are deferred to Appendix.

Results. Table 1 reports the overall performance of the comparison models on eight simulation datasets with different configurations. The comparison models include: Linear Prediction (Linear) (Satorras et al., 2021), SE3-Transformer (SE(3)-Tr.) (Fuchs et al., 2020), Radial-Field (RF) (Köhler et al., 2019), GNN and EGNN (Satorras et al., 2021). For all these models, we employ the codes and architectures implemented by Satorras et al. (2021).

From Table 1, we have the following observations:

- Clearly, EGHN surpasses all other approaches in all cases, demonstrating the general superiority of its design.
- Increasing the number of complexes (M) or the number of particles (N) always increases the complexity of the input system, but this does not necessarily hinder the performance of EGHN. For example, in both the single-system and multiple-system cases, EGHN even performs better when the system is changed from $(5, 5)$ to $(5, 10)$ and $(10, 10)$. We conjecture that, with more particles/complexes, larger systems also provide more data samples to enhance the training of EGHN.
- When increasing the diversity of systems (J) by switching from the single-system mode to multi-system mode, the performance of EGHN only drops slightly, indicating its adaptability to various scenarios.

Meanwhile, we visualize in Figure 3 the predictions of EGNN and our EGHN on the $(3, 3, 1)$ scenario. We can find that EGHN predicts the movements of the rigid objects more accurately than EGNN, especially for the large objects. In the right sub-figure, we also display the pooling results of EGHN, outputted by the score matrix of the final E-Pool layer. It is observed that EGHN is able to detect the correct cluster for each particle. This is interesting and it can justify the worth of designing hierarchical architecture for multi-body system modeling.

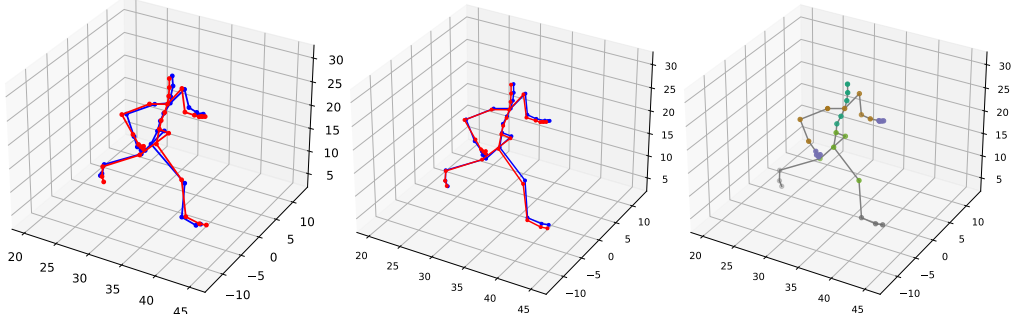


Figure 4: Visualization on the motion capture dataset. *Left*: the prediction of EGNN. *Middle*: the prediction of EGHN. *Right*: the pooling results of EGHN with each color indicating a cluster. In the left and middle figure, ground truth in **red**, and prediction in **blue**. Best viewed by colour printing and zooming in.

4.2 Motion Capture

We further evaluate our model on CMU Motion Capture Database (CMU, 2003). We primarily focus on two activities, namely *walking* (Subject #35) (Kipf et al., 2018) and *running* (Subject #9). With regard to walking, we leverage the random split adopted by Huang et al. (2022), which includes 200 frame pairs for training, 600 for validation, and another 600 for testing. As for running, we follow a similar strategy and obtain a split with 200/240/240 frame pairs. The interval between each pair is 30 frames in both scenarios. In this task the joints are edges and their intersections are the nodes.

Implementation details. As discussed in Fuchs et al. (2020), many real-world tasks, including our motion capture task here, break the Euclidean symmetry along the gravity axis (z -axis), and it is beneficial to make the equivariant models aware of where the top is. To this end, we augment the node feature by the coordinate of the z -axis, resulting in models that are height-aware while still equivariant horizontally. Since the interaction of human body works along the joints, we propose to involve the edge in A_{global} if it connects the nodes within two hops in \mathcal{G} . For the number of clusters K , we empirically find that $K = 5$ yields promising results for both walking and running.

Table 2: Prediction error ($\times 10^{-2}$) on the motion capture dataset. Results averaged across 3 runs.

	Subject #35 Walk	Subject #9 Run
GNN	36.1 ± 1.5	66.4 ± 2.2
RF	188.0 ± 1.9	521.3 ± 2.3
TFN	32.0 ± 1.8	56.6 ± 1.7
SE(3)-Tr.	31.5 ± 2.1	61.2 ± 2.3
EGNN	28.7 ± 1.6	50.9 ± 0.9
GMN	21.6 ± 1.5	44.1 ± 2.3
EGHN	8.5 ± 2.2	25.9 ± 0.3

Results. Table 2 summarizes the whole results of all models on two subjects. Here, we supplement an additional baseline GMN Huang et al. (2022) for its promising performance on this task. Excitingly, EGHN outperforms all compared baselines by a large margin on both activities. Particularly, on Subject #35, the prediction error of EGHN is 8.5×10^{-2} , which is much lower than that of the best baseline, *i.e.*, GMN (21.6×10^{-2}).

To investigate why EGHN works, we depict the skeletons estimated by both EGNN and EGHN on Subject #9 in Figure 4. It shows that EGHN is able to capture more fine-grained details on certain parts (*e.g.* the junction between the legs and the body) than EGNN. When we additionally visualize the pooling outcome in the right sub-figure, we interestingly find that EGHN is capable of classifying the two right-left hands into the same cluster even they are spatially disconnected. A similar result is observed for the arms and feet. This is reasonable as EGHN checks not only if two particles are spatially close to each other but also if they share the similar dynamics.

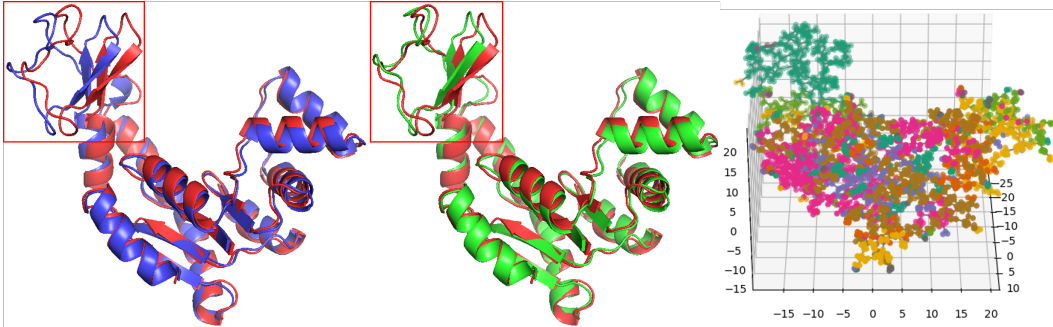


Figure 5: Visualization on the MDAnalysis dataset. *Left*: the prediction of EGNN. *Middle*: the prediction of EGHN. *Right*: the pooling results of EGHN with each color indicating a cluster. In the left and middle figure, ground truth in red, prediction for EGNN in blue, and prediction for EGHN in green. Best viewed by colour printing and zooming in.

4.3 Molecular Dynamics on Proteins

We adopt AdK equilibrium trajectory dataset (Seyler & Beckstein) via MDAnalysis toolkit (Richard J. Gowers et al., 2016) to evaluate our hierarchical model. The AdK equilibrium trajectory dataset involves the MD trajectory of apo adenylyl kinase simulated with explicit water and ions in NPT at 300 K and 1 bar. The atoms’ positions of the protein are saved every 240 ps for a total of 1.004 μ s as frames. The atoms’ velocities of the protein at each frame are computed by subtracting the positions to the next frame’s positions. Our goal here is to predict the future positions and velocities of the atoms in the protein given the current system state.

Implementation details. We split the dataset into train/validation/test sets along the timeline that contain 2481/827/878 frame pairs respectively. We choose $T = 15$ as the span between the input and prediction frames. We ignore the hydrogen atoms to focus on the prediction of large atoms. We further establish the global adjacency matrix as the neighboring atoms within a distance of 6 \AA .

Results. We contrast the performance of EGHN against other two equivariant models: RF and EGNN, in Figure 6. Akin to the previous tasks, EGHN gains the lowest prediction error. Figure 5 visualizes the 3D protein structures predicted by EGNN and EGHN, where we observe that EGHN tracks the folding and dynamics of the protein more precisely than EGNN, particularly for the region around a “beta-sheet”. Besides, the right sub-figure demonstrates the clustering result by EGHN in the all-atom molecular format. It suggests that EGHN discovers local repetitive sub-structures of the protein; for instance, it has detected the free radicals (colored as green on the top-left corner) probably owing to their synergistic behavior during the MD process.

4.4 Ablation Studies

We investigate the necessity of our proposed components on the motion capture dataset. We study the following questions: **1.** How will the performance of EGHN change, if we vary the number of clusters (K)? **2.** What if we remove the equivariance by replacing EMMP with typical MPNN? **3.** How does the connectivity loss (the second term in Eq. 17) help? **4.** How about using the same adjacency matrix for all EMMP instead of distinguishing them as A_{global} in the external EMMPs and A_{local} in internal EMMPs as discussed in § 3.5?

The results of all ablations are recorded in Table 3. We have the following findings.

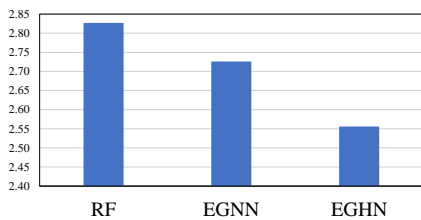


Figure 6: The prediction error of equivariant models on the protein molecular dynamics dataset.

- We modify the number of clusters K from 5 to 3 and 8, both of which yield worse performance. Specifically, we find that decreasing K on “Run” results in a larger degradation of performance, possibly because the activity “Run” is with complicated kinematics and it will be more difficult to learn if the joints are shared across a too small number of clusters.
- Without equivariance, EGHN become much worse, which justifies that maintaining equivariance is crucial in this task.
- By dropping the connectivity loss, we observe a larger prediction error. This justifies the necessity of using the connectivity loss to focus more on intra-cluster connections against the inter-cluster edges.
- When we apply A_{global} or A_{local} for all EMMPs, the performance drops dramatically, implying that the external EMMPs and internal EMMPs play different roles in our architecture, and they should be equipped with different adjacency matrices to model the interactions between particles of different scopes.

Overall, the results in Table 3 support the validity of our design.

Table 3: Ablation studies on the motion capture dataset. The numbers are the prediction error ($\times 10^{-2}$).

	Subject #35	Subject #9
	Walk	Run
EGHN ($K = 5$)	8.5	25.9
EGHN ($K = 3$)	10.1	41.4
EGHN ($K = 8$)	14.9	26.8
w/o Equivariance	19.7	40.9
w/o Connectivity loss	10.5	28.8
A_{global} only	17.4	31.5
A_{local} only	16.8	33.5

5 Conclusion

In this paper, we have proposed a novel framework dubbed Equivariant Graph Hierarchy-based Network (EGHN) to model and represent the dynamics of multi-body systems. To reveal the representation hierarchy, EGHN leverages E-Pool to group the low-level nodes into a fixed number of clusters, and these clusters encoding the substructures of the low-level nodes are considered as the nodes in the next layer. To accomplish the inverse process, we propose E-UpPool to restore the low-level information from the high-level systems with the aid of the clustering score matrix computing by the corresponding E-Pool layer. The fundamental layer of EGN lies in the generalized Equivariant Matrix Message Passing (EMMP) to characterize the topology and dynamics of each input system expressively. For the experimental evaluations on M-complex systems, Motion-Capture, and protein MD, our EGHN consistently outperforms other non-hierarchical EGNs as well as non-equivariant GNNs.

References

Battaglia, P. W., Pascanu, R., Lai, M., Rezende, D., and Kavukcuoglu, K. Interaction networks for learning about objects, relations and physics. *arXiv preprint arXiv:1612.00222*, 2016.

Cangea, C., Veličković, P., Jovanović, N., Kipf, T., and Liò, P. Towards sparse hierarchical graph classifiers, 2018.

CMU. Carnegie-mellon motion capture database. 2003. URL <http://mocap.cs.cmu.edu>.

Deng, C., Zhao, Z., Wang, Y., Zhang, Z., and Feng, Z. Graphzoom: A multi-level spectral approach for accurate and scalable graph embedding. In *International Conference on Learning Representations*, 2020. URL <https://openreview.net/forum?id=r11G00EKDH>.

Finzi, M., Stanton, S., Izmailov, P., and Wilson, A. G. Generalizing convolutional neural networks for equivariance to lie groups on arbitrary continuous data. In *International Conference on Machine Learning*, pp. 3165–3176. PMLR, 2020.

Fuchs, F. B., Worrall, D. E., Fischer, V., and Welling, M. Se (3)-transformers: 3d roto-translation equivariant attention networks. *arXiv preprint arXiv:2006.10503*, 2020.

Greydanus, S., Dzamba, M., and Yosinski, J. Hamiltonian neural networks. In Wallach, H., Larochelle, H., Beygelzimer, A., d'Alché-Buc, F., Fox, E., and Garnett, R. (eds.), *Advances in Neural Information Processing Systems*, volume 32. Curran Associates, Inc., 2019. URL <https://proceedings.neurips.cc/paper/2019/file/26cd8ecadce0d4efd6cc8a8725cbd1f8-Paper.pdf>.

Hu, F., Zhu, Y., Wu, S., Wang, L., and Tan, T. Hierarchical graph convolutional networks for semi-supervised node classification. In *Proceedings of the Twenty-Eighth International Joint Conference on Artificial Intelligence, (IJCAI)*, 2019. URL <https://arxiv.org/abs/1902.06667>.

Huang, W., Han, J., Rong, Y., Xu, T., Sun, F., and Huang, J. Constrained graph mechanics networks. In *International Conference on Learning Representations*, 2022. URL <https://openreview.net/forum?id=SHbhHHfePhP>.

Hutchinson, M. J., Le Lan, C., Zaidi, S., Dupont, E., Teh, Y. W., and Kim, H. Lietransformer: equivariant self-attention for lie groups. In *International Conference on Machine Learning*, pp. 4533–4543. PMLR, 2021.

Kipf, T., Fetaya, E., Wang, K.-C., Welling, M., and Zemel, R. Neural relational inference for interacting systems. *arXiv preprint arXiv:1802.04687*, 2018.

Köhler, J., Klein, L., and Noé, F. Equivariant flows: sampling configurations for multi-body systems with symmetric energies. *arXiv preprint arXiv:1910.00753*, 2019.

Lee, J., Lee, I., and Kang, J. Self-attention graph pooling. In *Proceedings of the 36th International Conference on Machine Learning*, 09–15 Jun 2019.

Mrowca, D., Zhuang, C., Wang, E., Haber, N., Fei-Fei, L., Tenenbaum, J. B., and Yamins, D. L. Flexible neural representation for physics prediction. *arXiv preprint arXiv:1806.08047*, 2018.

Pfaff, T., Fortunato, M., Sanchez-Gonzalez, A., and Battaglia, P. W. Learning mesh-based simulation with graph networks. *arXiv preprint arXiv:2010.03409*, 2020.

Richard J. Gowers, Max Linke, Jonathan Barnoud, Tyler J. E. Reddy, Manuel N. Melo, Sean L. Seyler, Jan Domański, David L. Dotson, Sébastien Buchoux, Ian M. Kenney, and Oliver Beckstein. MDAnalysis: A Python Package for the Rapid Analysis of Molecular Dynamics Simulations. In Sebastian Benthall and Scott Rostrup (eds.), *Proceedings of the 15th Python in Science Conference*, pp. 98 – 105, 2016. doi: 10.25080/Majora-629e541a-00e.

Sanchez-Gonzalez, A., Bapst, V., Cranmer, K., and Battaglia, P. Hamiltonian graph networks with ode integrators. *arXiv preprint arXiv:1909.12790*, 2019.

Sanchez-Gonzalez, A., Godwin, J., Pfaff, T., Ying, R., Leskovec, J., and Battaglia, P. Learning to simulate complex physics with graph networks. In *International Conference on Machine Learning*, pp. 8459–8468. PMLR, 2020.

Satorras, V. G., Hoogeboom, E., and Welling, M. E(n) equivariant graph neural networks. *arXiv preprint arXiv:2102.09844*, 2021.

Seyler, S. and Beckstein, O. Molecular dynamics trajectory for benchmarking md-analysis, 6 2017. URL: https://figshare.com/articles/Molecular_dynamics_trajectory_for_benchmarking_MDAnalysis/5108170, doi, 10:m9.

Thomas, N., Smidt, T., Kearnes, S., Yang, L., Li, L., Kohlhoff, K., and Riley, P. Tensor field networks: Rotation-and translation-equivariant neural networks for 3d point clouds. *arXiv preprint arXiv:1802.08219*, 2018.

Ummenhofer, B., Prantl, L., Thuerey, N., and Koltun, V. Lagrangian fluid simulation with continuous convolutions. In *International Conference on Learning Representations*, 2019.

Xing, Y., He, T., Xiao, T., Wang, Y., Xiong, Y., Xia, W., Wipf, D., Zhang, Z., and Soatto, S. Learning hierarchical graph neural networks for image clustering. In *Proceedings of the IEEE/CVF International Conference on Computer Vision (ICCV)*, pp. 3467–3477, October 2021.

Ying, Z., You, J., Morris, C., Ren, X., Hamilton, W., and Leskovec, J. Hierarchical graph representation learning with differentiable pooling. In Bengio, S., Wallach, H., Larochelle, H., Grauman, K., Cesa-Bianchi, N., and Garnett, R. (eds.), *Advances in Neural Information Processing Systems*, volume 31. Curran Associates, Inc., 2018. URL <https://proceedings.neurips.cc/paper/2018/file/e77dbaf6759253c7c6d0efc5690369c7-Paper.pdf>.

Yu, J., Xu, T., Rong, Y., Bian, Y., Huang, J., and He, R. Graph information bottleneck for subgraph recognition. In *International Conference on Learning Representations*, 2020.

A Hyper-parameters

For the baselines, we leverage the codebase maintained by (Satorras et al., 2021). We tune the hyper-parameters around the suggested hyper-parameters as specified in (Huang et al., 2022) for the baselines. Specifically, for GNN, RF and EGN, we tune the learning rate from [1e-4, 5e-4, 1e-3], weight decay [1e-10, 1e-8], batch size [50, 100, 200], hidden dim [32, 64, 128] and the number of layers [2, 4, 6, 8]. For TFN and SE(3)-Transformer, we set the degree to 2 due to memory limitation, and select the learning rate from [5e-4, 1e-3, 5e-3], weight decay [1e-10, 1e-8], batch size [25, 50, 100], hidden dim [32, 64] and the number of layers [2, 4]. We use an early-stopping of 50 epochs for all methods.

For EGHN, on simulation dataset, we use batch size 50, and the number of clusters the same as the complexes in the dataset. On motion capture, we use batch size 12, and the number of clusters $K = 5$ on both datasets. On MD dataset, we use batch size 8, and the number of clusters $K = 15$. Table 4 depicts the rest of tuned hyper-parameter configurations.

Table 4: Hyper-parameters of EGHN.

Dataset	learning rate	λ	weight decay	Encoder EMMP Layer	Decoder EMMP Layer
(3, 3, 1)	0.0005	4	1e-4	4	2
(3, 3, 5)	0.001	4	1e-4	4	2
(5, 5, 1)	0.0003	2	1e-6	4	2
(5, 5, 5)	0.001	0.1	1e-12	4	2
(5, 10, 1)	0.0001	4	1e-4	2	2
(5, 10, 5)	0.0005	4	1e-4	4	2
(10, 10, 1)	0.0005	2	1e-6	4	2
(10, 10, 5)	0.0003	1	1e-8	4	2
Mocap Walk	0.0004	1	1e-6	2	2
Mocap Run	0.0003	1	1e-6	4	1
MD	0.0002	0.5	1e-4	3	2

B More Visualization

In this section, we provide more visualization results. Figure 7, Figure 8 and Figure 9 illustrate more visualization examples on (5, 5, 1) of the simulation dataset, walking on the motion capture dataset, and the MD dataset, respectively.

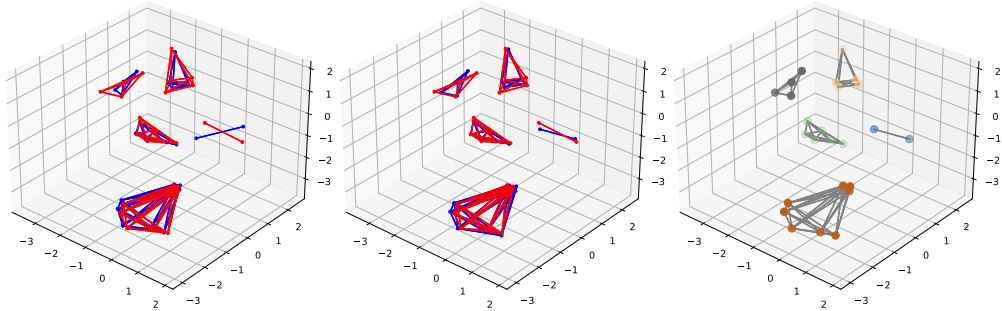


Figure 7: *Left*: the prediction of EGNN. *Middle*: the prediction of EGHN. *Right*: the pooling results of EGHN with each color indicating a cluster. Ground truth in red, and prediction in blue. Best viewed by colour printing and zooming in.

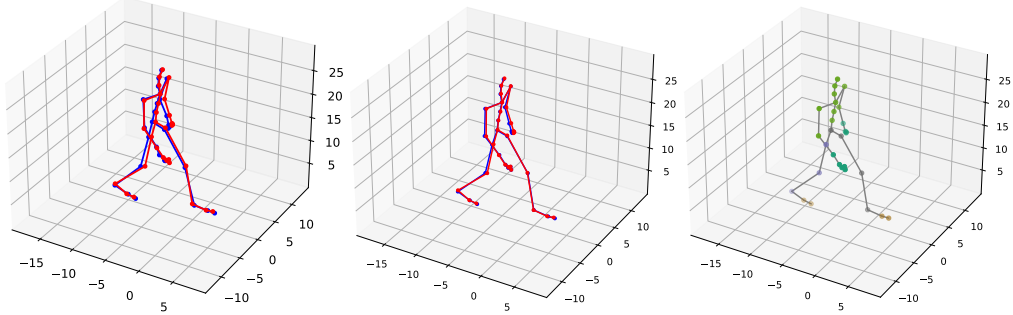


Figure 8: *Left*: the prediction of EGNN. *Middle*: the prediction of EGHN. *Right*: the pooling results of EGHN with each color indicating a cluster. Ground truth in red, and prediction in blue. Best viewed by colour printing and zooming in.

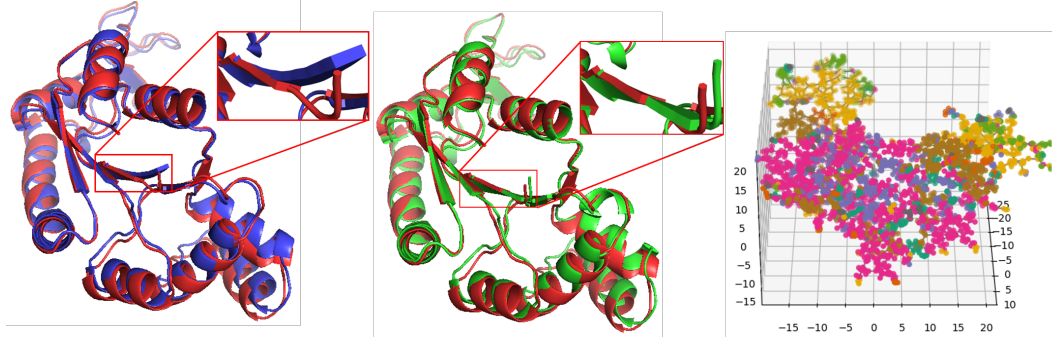


Figure 9: *Left*: the prediction of EGNN. *Middle*: the prediction of EGHN. *Right*: the pooling results of EGHN with each color indicating a cluster. In the left and middle figure, ground truth in red, prediction for EGNN in blue, and prediction for EGHN in green. Best viewed by colour printing and zooming in.

C Learning curve

We provide the learning curve of EGHN and EGNN on (3, 3, 1) of the simulation dataset. It is illustrated that EGHN converges faster and the corresponding testing loss is lower as well, yielding better performance than EGNN.

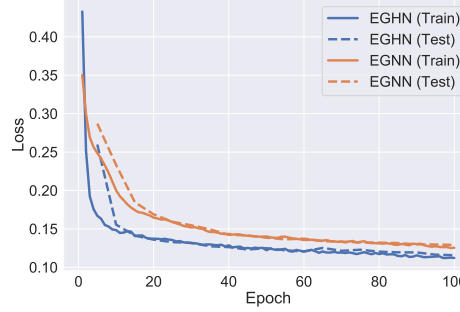


Figure 10: The learning curves of EGHN and EGNN on (3, 3, 1) of the simulation dataset.